JSS Focus Issue on Gallium Oxide Based Materials and Devices

Valence and Conduction Band Offsets for InN and III-Nitride Ternary Alloys on (−201) Bulk β-Ga_2O_3

Chaker Fares,[1,*,z] Marko J. Tadjer,[2] Jeffrey Woodward,[3] Neeraj Nepal,[2] Michael A. Mastro,[2] Charles R. Eddy Jr.,[2] Fan Ren,[1,] and Stephen J. Pearton[1,**]**

[1] *University of Florida, Gainesville, Florida 32611, USA*
[2] *Naval Research Laboratory, Washington, DC, USA*
[3] *American Society for Engineering Education Postdoctoral Fellow, Residing at NRL, Washington, DC, USA*

Valence and conduction band offsets of the InN/β-Ga_2O_3 type-I heterojunction have been determined to be −0.55 ± 0.11 eV and −3.35 ± 0.11 eV, respectively, using X-ray photoelectron spectroscopy. The InN layers were grown using atomic layer epitaxy on (−201) oriented commercial β-Ga_2O_3 substrates. Combining this data with published band offsets for the GaN and AlN heterojunctions to β-Ga_2O_3 has allowed us to predict the band offsets for the AlGaN, AlInN, and InGaN ternary alloys to β-Ga_2O_3. The conduction band offsets for InGaN and AlInN to β-Ga_2O_3 increased for high In concentration and, similarly, the valence band offsets for AlGaN and AlInN to β-Ga_2O_3 decreased at high Al concentration.

 [DOI: 10.1149/2.0281907jss]

Manuscript submitted December 28, 2018; revised manuscript received March 8, 2019. Published March 16, 2019. *This paper is part of the JSS Focus Issue on Gallium Oxide Based Materials and Devices.*

Gallium oxide has recently experienced resurgent interest as a viable material for power electronic devices. Long known as an ultra-wide bandgap semiconductor (E_G = 4.7–4.9 eV), recent advances in growth and commercialization of low-cost, large-area substrates as well as controlled-doping epitaxy have provided device engineers with a new material platform to further push the Baliga Figure of Merit beyond that of GaN and SiC ($BFOM_{Ga2O3}$ = 3444).[1–4] Demonstrations of n-type Ga_2O_3 doped over a wide range have suggested that both low on resistance and high blocking voltage are achievable with this material.[5–9] In particular, n^+-doped Ga_2O_3 has been demonstrated using pulsed laser deposition (PLD), low pressure chemical vapor deposition (LPCVD), and molecular beam epitaxy (MBE) in what have been important steps toward demonstrating the potential of this material for future ultra-wide bandgap electronics.[10–13] Due to the challenge of making low-resistance ohmic contacts to wide bandgap semiconductors, local doping enhancement by ion implantation, plasma exposure, or the addition of a low bandgap interlayer must be used. Out of several low bandgap materials, InN is a strong candidate due to its ability to be grown highly n^+ which could allow its function as a regrown barrier for an ohmic contact to Ga_2O_3.[14,15]

In this work, we have explored InN deposition on β-Ga_2O_3 and measured the band offsets of this heterojunction. The band offsets of InN grown on β-Ga_2O_3 are used to report an experimental band diagram of this heterojunction. Band offsets have been reported for most relevant oxides on Ga_2O_3 in search of candidate gate dielectrics for ultra-wide bandgap electronics.[16–26] In addition, common semiconductor heterojunctions have been reported as well, including Si, SiC, GaN, AlN, and IZGO.[27–32] Measuring band offsets for the InN/β-Ga_2O_3 heterojunction is thus complementary to the reported results for the other III-Nitride materials AlN and GaN. Particularly for AlN, Sun et al. have reported β-Ga_2O_3 growth on AlN substrate, whereas Chen et al. have deposited AlN by plasma and thermal atomic layer deposition on β-Ga_2O_3.[31,32] In search of a suitable p-type semiconductor in the absence of p-type doped Ga_2O_3, CuI growth on Ga_2O_3 by iodination of Cu, as well as band offsets, have been recently reported.[33,34] Figure 1 summarizes these reported band offsets to Ga_2O_3. Furthermore, reports of band offsets to $(Al_xGa_{1-x})_2O_3$ have begun to emerge, with CuI and SiO_2 already reported.[34,35]

Experimental

Samples of 8 × 8 mm size were diced out from a commercial (−201) β-Ga_2O_3 unintentionally doped substrate. The wafers were cleaned in sequential 5-minute ultrasonic baths of acetone, isopropanol, and deionized water. The InN films were grown at 320°C by plasma-assisted atomic layer epitaxy (ALEp) using a Veeco/Cambridge Nanotech (CNT) Fiji 200. In preparation for InN growth, an additional in situ hydrogen plasma clean of the wafers was performed at 320°C with constant ultrahigh purity (UHP) argon flows of 30 sccm and 100 sccm through the metallorganic precursor manifold and plasma source, respectively. The plasma clean consisted of 10 sequential 20 second plasma exposures at 300 W forward power separated by 5 second argon purges. During these exposures, 50 sccm of UHP hydrogen was flowed through the plasma source in addition to the argon.

Upon completion of the hydrogen plasma clean, the constant argon flows were reduced to 15 sccm and 25 sccm through the

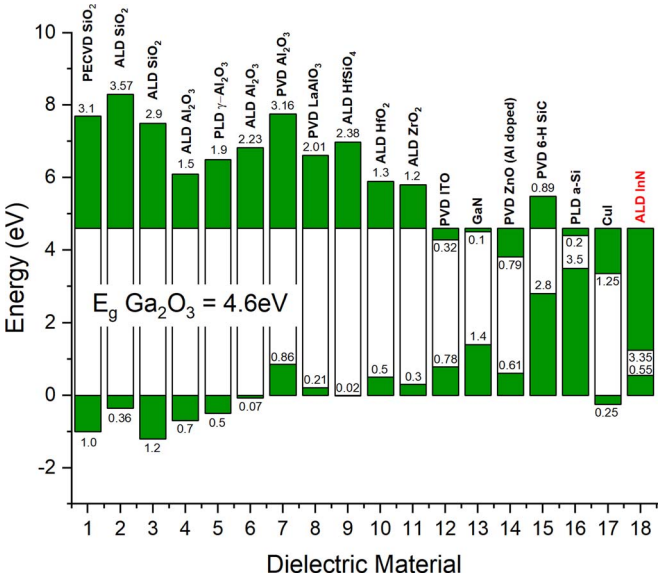

Figure 1. Reported band offsets for various dielectrics and contact materials on Ga_2O_3.

*Electrochemical Society Member.
**Electrochemical Society Fellow.
[z]E-mail: c.fares@ufl.edu

Table I. Summary of measured core levels in these experiments (eV).

Reference Ga_2O_3 substrate				Thick InN reference on Ga_2O_3				Thin InN on Ga_2O_3	
Core Level	VBM	Core Level Peak	Core - VBM	Core Level	VBM	Core Level Peak	Core - VBM	Δ Core Level Ga $2p_{3/2}$ – In $3d_{5/2}$	Valence Band Offset
Ga $2p_{3/2}$	3.20	1118.10	1114.90	In $3d_{5/2}$	1.35	443.9	442.55	672.9	-0.55 ± 0.11 eV

precursor manifold and plasma source, respectively. The reactor pressure at these flows was 133 millitorr. Each ALEp growth cycle consisted of a 0.12 second pulse of trimethylindium, followed by an 8–10 second argon purge, a 25 second plasma nitridation at 300 W forward power with 50 sccm UHP nitrogen added to the argon flow, and a final 10 second argon purge. For the last 5 seconds of each plasma nitridation, 5 sccm of hydrogen was introduced through the plasma source to supplement the nitrogen and argon for the purpose of reducing impurities and improving film quality. A sequence of 30 growth cycles was used to grow the thin InN film, whereas 600 cycles were used for the thick film, corresponding to InN film thickness of about 2 nm and 40 nm, respectively. TEM and surface characterization of ALE-grown InN that confirm the smooth morphology have been detailed in the literature.[14,15] Using this growth technique, we have previously demonstrated high quality, very flat, 5 nm thick InN films with mobility of 50 cm^2/Vs, higher than that of 1.3 μm thick InN grown by molecular beam epitaxy.[36,37]

XPS was performed using a monochromatic, Al X-ray source in an ULVAC PHI system with a source power of 300 W. Charge compensation was achieved with a dual beam charge neutralization system with simultaneous low-energy electron and ion beams.[20] The adventitious carbon (C-C) line in the C 1s spectra at 284.8 eV was used for charge correction. The samples and electron analyzers were electrically grounded to provide a common reference Fermi level. We did not observe any effects due to differential charging.[38] Reflection electron energy loss spectroscopy (REELS) was used for measurement of the bandgap of the Ga_2O_3, using a 1 kV electron beam and the hemispherical electron analyzer.[39]

Results and Discussion

The thick InN films were utilized for valence band maximum (VBM) measurements of the InN film. The thinner InN films were necessary for the X-Ray photoelectron spectroscopy measurement of core valence electron difference between InN and Ga_2O_3. Finally, the VBM of Ga_2O_3 was measured on a bare Ga_2O_3 reference substrate by XPS as well. These results are summarized in Table I. The detailed XPS characterization and band diagram determination are discussed in the next section.

The XPS scans of the two InN samples, along with a control Ga_2O_3 substrate, are shown in Fig. 2. Signature peaks with high intensity from the expected elements (Ga, O, In, N, and C) were present. The Ga 2p core shell peak, clearly visible on the reference Ga_2O_3 scan, was absent from the InN scans. The O 1s peak was greatly suppressed in the InN scans but not completely absent, indicating that a small amount of O was still present on the surface of the InN films despite storing the samples in vacuum. Within the Ga_2O_3 survey scan, the peaks shown are the Ga-3d peak with binding energy of about 20.5 eV, Ga-3p around 105 eV, Ga-3s at about 160 eV, and there is the Ga-2p region around 1118.0 eV. The additional features seen between 400 and 600 eV are Auger lines which can strongly interfere with the N-1s signal having BE of about 400 eV for the samples covered with InN. Therefore, detailed spectra taken with a low-pass energy was utilized to determine peak location in this region. For the 1.5 nm InN film on Ga_2O_3, the intense peak around 20 eV is primarily due to the In-4d peak. A small amount of oxidation was expected due to the brief exposure of the InN films to atmosphere. As the growth process for InN on an oxide substrate continues to be optimized, we note that any potential O content in the InN, particularly at the interface, could significantly affect the measured band offsets and would be difficult to detect with spectroscopic methods alone.

In a non-destructive method based on XPS first reported by Kraut et al., the band diagram of a heterojunction of two dissimilar materials can be determined by measuring the core energy levels and the valence band maxima of each material.[38] Based on this information, the valence band offset between the two materials can be calculated with high degree of precision. For the case of the InN-Ga_2O_3 heterostructure, Kraut's method defines the valence band offset as shown in Eq. 1,

$$\Delta E_V = \left(E_{core}^{Ga2O3} - E_{VBM}^{Ga2O3}\right) - \left(E_{core}^{InN} - E_{VBM}^{InN}\right) - \left(E_{core}^{Ga2p} - E_{core}^{In3d}\right) \quad [1]$$

where E_{VBM}^{Ga2O3} was determined from the VBM measurement on the control Ga_2O_3 substrate (Fig. 3a) and E_{VBM}^{InN} was determined from the VBM spectrum of the thick InN film (Fig. 3b). Each VBM experimental determination was based on the intersection of the flat XPS energy approaching the valence band of the material and the linear fit of the leading valence band edge in the XPS data. Then, E_{core}^{Ga2O3} and E_{core}^{InN} were determined from the vacuum-core delta regions of the XPS spectra of the thin InN film (Fig. 4a) and the thick InN film (Fig. 4b). Finally, the high resolution XPS spectra for the InN to Ga_2O_3 core delta regions (Fig. 5) yielded the value of 672.9 eV for $E_{core}^{Ga2p} - E_{core}^{In3d}$. Using these values (summarized in Table I), the valence band offset ΔE_V for this heterojunction was calculated to be -0.55 ± 0.11 eV using Eq. 1. We note that this band offset is significantly different compared to the one expected for InN grown on a III-Nitride surface such as GaN (+0.58 eV).[40] In fact, our measured valence band offset for InN was similar to the the theoretical valence band offset for In_2O_3/Ga_2O_3, as recently reported by Swallow et al.[41] It is worth pointing out that measured valence bands for AlN and Al_2O_3, deposited by ALD on (−201) β-Ga_2O_3 by two different groups, were similar as well: -0.09 ± 0.1 eV for PEALD AlN and 0.07 ± 0.2 eV for ALD Al2O3.[17,31] While interfacial O was likely present in our films, preliminary depth-resolved XPS profiling did not indicate significant O content in our films, and as our growth substrate was an oxide the interfacial O content was impossible to quantify. We would reasonably expect the valence band offset for InN to Ga_2O_3 in future reports to increase by up to about 1 eV as the effect of interfacial O is eliminated.

To determine the conduction band offset in a heterojunction, prior knowledge of the bandgap of the two films is required. The bandgap of (−201) Ga_2O_3 was determined to be 4.6 eV from the REELS spectrum

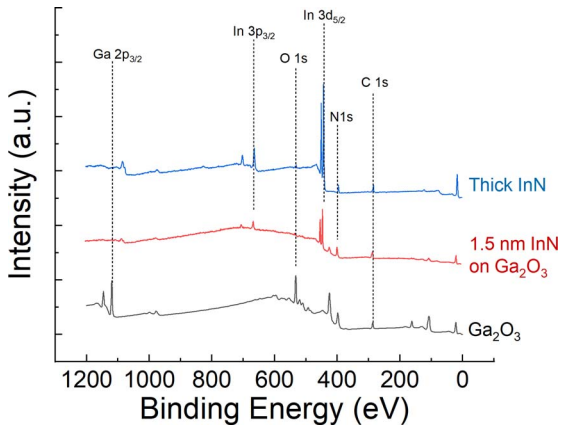

Figure 2. XPS survey scans of thick InN, 1.5 nm InN on Ga_2O_3, and a reference Ga_2O_3 sample, offset for readability. The intensity is in arbitrary units (a.u.).

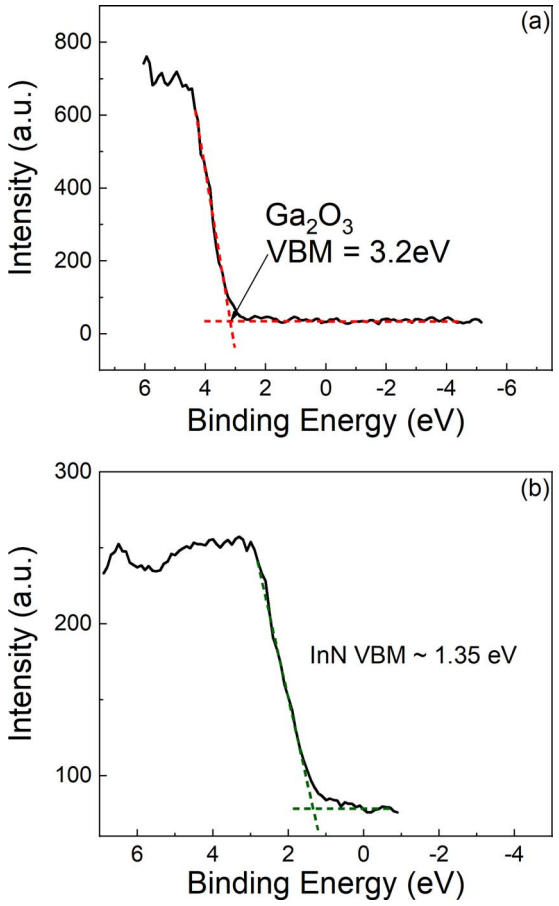

Figure 3. XPS spectra of core levels to valence band maximum (VBM) for (a) reference Ga_2O_3 and (b) Thick InN. The intensity is in arbitrary units (a.u.).

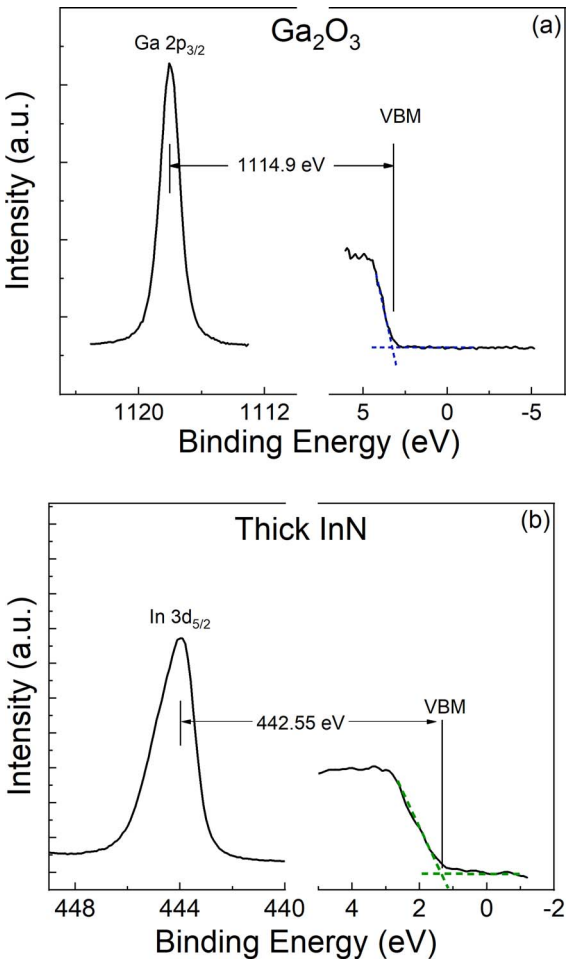

Figure 4. High resolution XPS spectra for the vacuum-core delta regions of (a) Ga_2O_3 and (b) thick InN. The intensity is in arbitrary units (a.u.).

of the control substrate (Fig. 6), showing reasonable consistency with prior reports.[42–45] The bandgap of InN was assumed to be 0.7 eV based on values reported in the literature by our group and others.[14,46] Thus, the conduction band offset ΔE_C, calculated to be -3.35 ± 0.11 eV based on the expression below.

$$\Delta E_C = E_G^{Ga2O3} - E_G^{InN} - |\Delta E_V| \quad [2]$$

Equation 2 is also evident from the band diagram of the InN-Ga_2O_3 heterostructure, presented in Fig. 7. Using the measured values for ΔE_C, ΔE_V, as well as the $Ga2p_{3/2}$ and $In3d_{5/2}$ core energy levels, a type-I band diagram was determined. This value for the conduction band offset is the largest reported among the reported semiconductor heterojunctions to β-Ga_2O_3 to-date.

Using the band offset data in this work and the published band offset values for GaN and AlN deposited on β-Ga_2O_3,[28,31] we have attempted to predict the band offsets for the ternary nitride alloys $Al_xGa_{1-x}N$, $Al_xIn_{1-x}N$, and $In_xGa_{1-x}N$ with β-Ga_2O_3. We note that atomic layer epitaxy is a particularly well-suited method for the development of such a generalized approach for band offset calculation as it is possible to cover the entire compositional range of a ternary nitride with this method, including the miscibility gap.[15] The bandgap of a ternary alloy $A_xB_{1-x}N$ was calculated using the following expression as a function of composition, x, and bandgap of the constituent binary compounds A and B:

$$E_{G,ABN}(x) = (1-x)E_{G,B} + xE_{G,A} - x(1-x)C \quad [3]$$

where C is the bowing parameter which accounts for the nonlinearity in the bandgap of the ternary alloy.[47–49] Since the bandgap is only used for the calculation of conduction band offsets (Eq. 2), valence band offsets of the ternary alloy $A_xB_{1-x}N$ were calculated using the valence band offsets of the binary compounds AN and BN as a function of composition, x.

$$\Delta E_{V,ABN} = \Delta E_{V,BN} - x\left(\Delta E_{V,BN} - \Delta E_{V,AN}\right) \quad [4]$$

The conduction band offset was subsequently determined using Eq. 2 where the bandgap of the ternary nitride calculated in Eq. 3 was

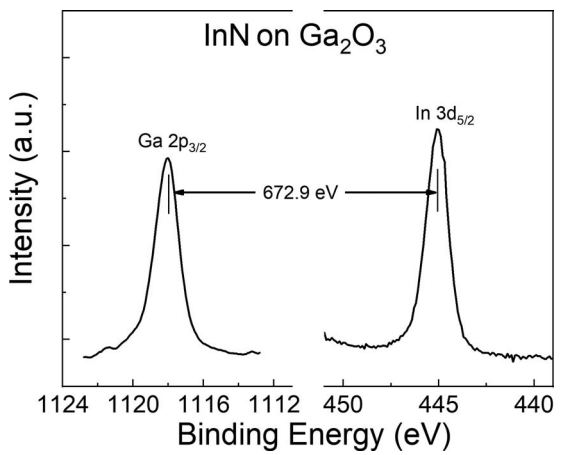

Figure 5. High resolution XPS spectra for the InN to Ga_2O_3 core delta regions, measured on the thin InN sample. The intensity is in arbitrary units (a.u.).

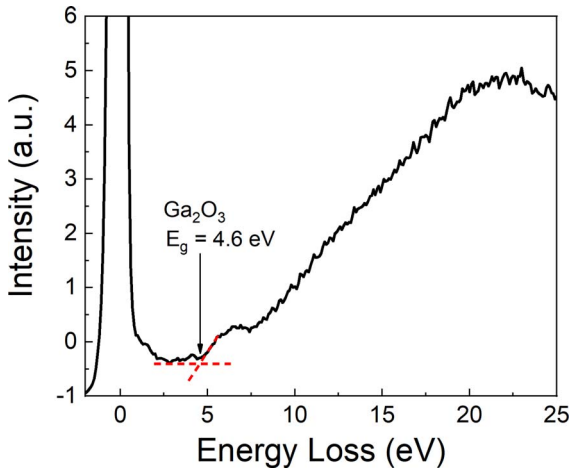

Figure 6. Bandgap of Ga_2O_3 determined by Reflection Electron Energy Loss Spectra. The intensities are in arbitrary units (a.u.)

substituted in place of the binary nitride gap,

$$\Delta E_{C,ABN} = E_G^{Ga2O3} - E_G^{ABN} - \left|\Delta E_{V,ABN}\right| \quad [5]$$

where bowing parameter values of 3 eV, 1 eV, and 4.7 eV were used for InGaN, AlGaN, and AlInN, respectively.[47,50] For consistency with the band offset data for GaN and AlN from the prior reports,[28,31] a bandgap energy of 4.9 eV was used for β-Ga_2O_3 for the purpose of this calculation. The resulting conduction and valence band offset curves for the ternary nitride alloys to β-Ga_2O_3 as a function of alloy composition x are presented in Fig. 8. As expected, valence band offsets were decreasing as the Al concentration increased in the AlGaN and AlInN alloys, whereas the conduction band offsets increased with In concentration in the AlInN and InGaN alloys. Accounting for the effects of epilayer thickness and strain, bandgap and bowing parameter temperature dependence, interface states, and other practical factors was beyond the scope of this study but can be reasonably expected to affect the band offsets of these heterojunctions.

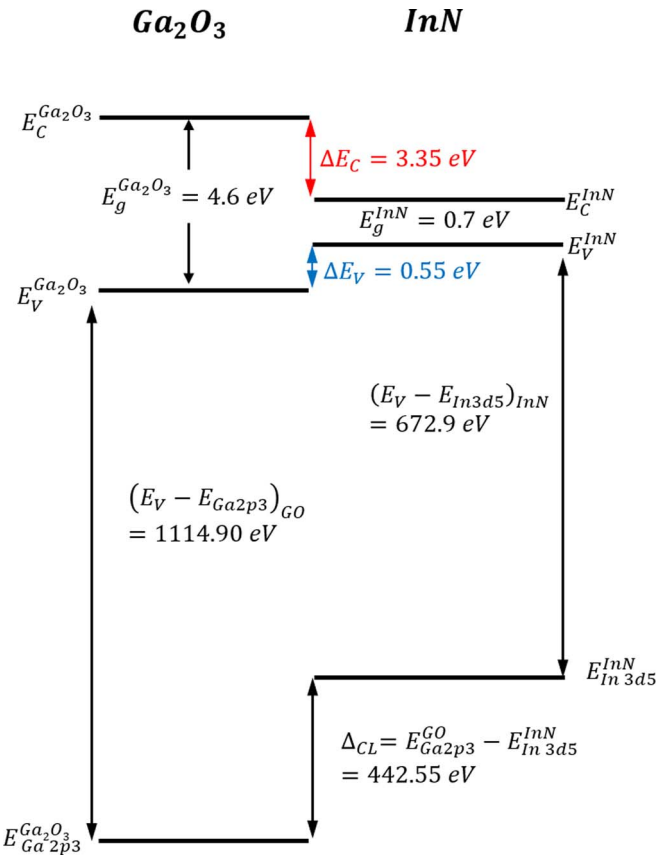

Figure 7. Band diagram for the InN-Ga_2O_3 heterostructure.

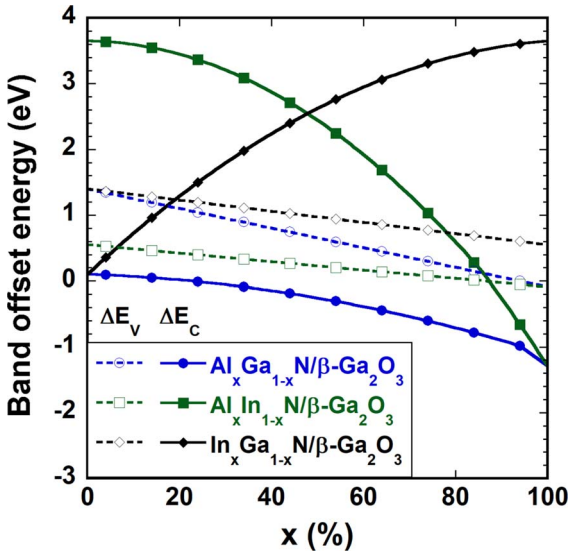

Figure 8. Calculated valence and conduction band offsets for ternary nitride alloys ($Al_xGa_{1-x}N$, $Al_xIn_{1-x}N$, $In_xGa_{1-x}N$) to β-Ga_2O_3 as a function of composition, x.

Conclusions

In summary, XPS measurements were performed on ALE-deposited InN films, whose quality has been previously shown to be similar to that of MBE-grown InN, on β-Ga_2O_3 substrates to determine the band offsets of this heterojunction. A type-I heterojunction was determined, with conduction band offset of -3.35 ± 0.11 eV and valence band offset of -0.55 ± 0.11 eV. This low valence band offset value was potentially attributed to unintentional O incorporation at the InN/Ga_2O_3 interface. Combined with published band offsets for the AlN and GaN heterojunctions to β-Ga_2O_3, we have then predicted the band offsets for the various ternary nitride alloys to this ultra-wide bandgap semiconductor. As Ga_2O_3 substrate technology matures, it could be potentially competitive as a substrate for III-Nitride electronic or optoelectronic heteroepitaxial devices, which are typically grown on sapphire or SiC substrates.

Acknowledgments

The project or effort depicted was partially sponsored by the Department of the Defense, Defense Threat Reduction Agency, HDTRA1-17-1-011, monitored by Jacob Calkins. The content of the information does not necessarily reflect the position or the policy of the federal government, and no official endorsement should be inferred. J.W. acknowledges postdoctoral fellowship from the American Society for Engineering Education. Research at the Naval Research Laboratory was supported by the Office of Naval Research. The authors are sincerely grateful to Dr. John Lyons (NRL) for insightful discussions.

ORCID

Chaker Fares https://orcid.org/0000-0001-9596-2381
Marko J. Tadjer https://orcid.org/0000-0002-2388-2937
Fan Ren https://orcid.org/0000-0001-9234-019X
Stephen J. Pearton https://orcid.org/0000-0001-6498-1256

References

1. H. Aida, K. Nishigchi, H. Takeda, N. Aota, K. Sunakawa, and Y. Yaguchi, *Jpn. J. Appl. Phys.*, **47**, 8506 (2008).
2. A. Kuramata, K. Koshi, S. Watanabe, Y. Yamakoka, T. Masui, and S. Yamakoshi, *Jpn. J. Appl. Phys.*, **55**, 1202A2 (2016).
3. M. Higashiwaki, K. Sasaki, A. Kuramata, T. Masui, and S. Yamakoshi, *Appl. Phys. Lett.*, **100**, 013504 (2012).
4. S. J. Pearton, J. Yang, P. H. Cary IV, F. Ren, J. Kim, M. J. Tadjer, and M. A. Mastro, *Appl. Phys. Rev.*, **5**, 011301 (2018).
5. H. Murakami, K. Nomura, K. Goto, K. Sasaki, K. Kawara, Q. T. Thieu, R. Togashi, Y. Kumagai, M. Higashiwaki, and A. Kuramata, *Appl. Phys. Expr.*, **8**, 015503 (2015).
6. D. Gogova, G. Wagner, M. Baldini, M. Schmidbauer, K. Irmscher, R. Schewski, Z. Galazka, M. Albrecht, and R. Fornari, *J. Cryst. Growth*, **401**, 665 (2014).
7. M. Baldini, M. Albrecht, A. Fiedler, K. Irmscher, R. Schewski, and G. Wagner, *ECS Jour. Solid State Sci. Technol.*, **6**, Q3040 (2017).
8. M. J. Tadjer, A. D. Koehler, J. A. Freitas Jr., J. C. Gallagher, M. C. Specht, E. R. Glaser, K. D. Hobart, T. J. Anderson, F. J. Kub, Q. T. Thieu, K. Sasaki, D. Wakimoto, K. Goto, S. Watanabe, and A. Kuramata, *Appl. Phys. Lett.*, **113**, 192102 (2018).
9. A. T. Neal, S. Mou, S. Rafique, H. Zhao, E. Ahmadi, J. S. Speck, K. T. Stevens, J. D. Blevins, D. B. Thomson, N. Moser, K. D. Chabak, and G. H. Jessen, *Appl. Phys. Lett.*, **113**, 062101 (2018).
10. S. Rafique, L. Han, M. J. Tadjer, J. A. Freitas Jr., N. A. Mahadik, and H. Zhao, *Appl. Phys. Lett.*, **108**, 182105 (2016).
11. S. Rafique, L. Han, A. T. Neal, S. Mou, M. J. Tadjer, R. H. French, and H. Zhao, *Appl. Phys. Lett.*, **109**, 132103 (2016).
12. K. D. Leedy, K. D. Chabak, V. Vasilyev, D. C. Look, J. J. Boeckl, J. L. Brown, S. E. Tetlak, A. J. Green, N. A. Moser, A. Crespo, D. B. Thomson, R. C. Fitch, J. P. McCandless, and G. H. Jessen, *Appl. Phys. Lett.*, **111**, 012103 (2017).
13. A. J. Green, K. D. Chabak, M. Baldini, N. Moser, R. Gilbert, R. C. Fitch Jr., G. Wagner, Z. Galazka, J. McCandless, A. Crespo, K. Leedy, and G. H. Jessen, *IEEE Electr. Dev. Lett.*, **38**, 790 (2017).
14. N. Nepal, N. Mahadik, L. O. Nyakiti, S. B. Qadri, M. J. Mehl, J. K. Hite, and C. R. Eddy Jr., *Cryst. Growth Des*, **13**, 1485 (2013).
15. N. Nepal, V. R. Anderson, J. K. Hite, and C. R. Eddy Jr., *Thin Solid Films*, **589**, 47 (2015).
16. P. H. Carey IV, F. Ren, D. C. Hays, B. P. Gila, S. J. Pearton, S. Jang, and A. Kuramata, *Appl. Surf. Sci.*, **442**, 179 (2017).
17. P. H. Carey IV, F. Ren, David C. Hays, B. P. Gila, S. J. Pearton, Soohwan Jang, and Akito Kuramata, *Vacuum*, **141**, 103 (2017).
18. P. H. Carey, F. Ren, D. C. Hays, B. P. Gila, S. J. Pearton, S. Jang, and A. Kuramata, *J. Vac. Sci. Technol. B.*, **35**, 041201 (2017).
19. P. Carey, F. Ren, D. C. Hays, B. P. Gila, S. J. Pearton, S. Jang, and A. Kuramata, *Vacuum*, **142**, 52 (2017).
20. P. Carey, F. Ren, D. C. Hays, B. P. Gila, S. J. Pearton, S. Jang, and A. Kuramata, *Jpn. J. Appl. Phys.*, **56**, 071101 (2017).
21. K. Konishi, T. Kamimura, M. H. Wong, K. Sasaki, A. Kuramata, S. Yamakoshi, and M. Higashiwaki, *Phys. Status Solidi B*, **253**, 623 (2016).
22. Y. Jia, K. Zheng, J. S. Wallace, J. A. Gardella, and U. Singisetti, *Appl. Phys. Lett.*, **106**, 102107 (2016).
23. T. Kamimura, K. Sasaki, M. H. Wong, D. Krishnamurthy, A. Kuramata, T. Masui, S. Yamakoshi, and M. Higashiwaki, *Appl. Phys. Lett.*, **104**, 192104 (2014).
24. M. Hattori, T. Oshima, R. Wakabayashi, K. Yoshimatsu, K. Sasaki, T. Masui, A. Kuramata, S. Yamakoshi, K. Horiba, H. Kumigashira, and A. Ohtomo, *Jpn. J. Appl. Phys.*, **55**, 1202B6 (2016).
25. V. D. Wheeler, D. I. Shahin, M. J. Tadjer, and C. R. Eddy Jr., *ECS J. Solid State Sci. Technol.*, **6**, Q3052 (2017).
26. S. M. Sun, W. J. Liu, Y. P. Wang, Y. W. Huan, Q. Ma, B. Zhu, S. D. Wu, W. J. Yu, R. H. Horng, C. T. Xia, Q. Q. Sun, S. J. Ding, and D. W. Zhang, *Appl. Phys. Lett.*, **113**, 031603 (2018).
27. Z. Chen, K. Hishihagi, X. Wang, K. Saito, T. Tanaka, M. Nishio, M. Arita, and Q. Guo, *Appl. Phys. Lett.*, **109**, 102106 (2016).
28. W. Wei, Z. Qin, S. Fan, Z. Li, K. Shi, Q. Zhu, and G. Zhang, *Nanoscale Res. Lett*, **7**, 562 (2012).
29. S. H. Chang, Z. Z. Chen, W. Huang, X. C. Liu, B. Y. Chen, Z. Z. Li, and E. W. Shi, *Chin. Phys. B.*, **20**, 116101 (2011).
30. Y.-W. Huan, X.-L. Wang, W.-J. Liu, H. Dong, S.-B. Long, S.-M. Sun, J.-G. Yang, S.-D. Wu, W.-J. Yu, R.-H. Horng, C.-T. Xia, H.-Y. Yu, H.-L. Lu, Q.-Q. Sun, S.-J. Ding, and D. W. Zhang, *J. Jour. Appl. Phys.*, **57**, 100312 (2018).
31. J. X. Chen, J. J. Tao, H. P. Ma, H. Zhang, J. J. Feng, W. J. Liu, C. Xia, H. L. Lu, and D. W. Zhang, *Appl. Phys. Lett.*, **112**, 261602 (2018).
32. H. Sun, C. G. Torres Castanedo, K. Kiu, K.-H. Li, W. Guo, R. Lin, X. Liu, J. Li, X. Li, J. X. Chen, J. J. Tao, H. P. Ma, H. Zhang, J. J. Feng, W. J. Liu, C. Xia, H. L. Lu, and D. W. Zhang, *Appl. Phys. Lett.*, **112**, 261602 (2018).
33. A. D. Koehler et al., Compound Semiconductor Week, June 1, 2018, Boston MA.
34. C. Fares, F. Ren, D. C. Hays, B. P. Gila, M. J. Tadjer, K. D. Hobart, and S. J. Pearton, *Appl. Phys. Lett.*, **113**, 182101 (2018).
35. C. Fares, F. Ren, E. Lambers, D. C. Hays, B. P. Gila, and S. J. Pearton, *J. Vac. Sci. Technol. B*, **36**, 061207 (2018).
36. N. Nepal, V. R. Anderson, S. D. Johnson, B. P. Downey, D. J. Meyer, A. DeMasi, Z. R. Robinson, K. F. Ludwig, and C. R. Eddy, *J. Vac. Sci. Technol. A*, **35**, 031504 (2017).
37. S.-Y. Kuo, F.-I Lai, W.-C. Chen, W.-T. Lin, C.-N. Hsiao, H.-I. Lin, and H.-C. Pan, *Diamond and Relat. Mater.*, **20**, 1188 (2011).
38. E. A. Kraut, R. W. Grant, J. R. Waldrop, and S. P. Kowalczyk, *Phys. Rev. Lett.*, **44**, 1620 (1980).
39. H. C. Shin, D. Tahir, S. Seo, Y. R. Denny, S. K. Oh, H. J. Kang, S. Heo, J. G. Chung, J. C. Lee, and S. Tougaard, *Surf. Interface Anal.*, **44**, 623 (2012).
40. P. D. C. King, T. D. Veal, C. E. Kendrick, L. R. Bailey, S. M. Durbin, and C. F. McConville, *Phys. Rev. B*, **78**, 033308 (2008).
41. J. E. N. Swallow, J. B. Varley, L. A. H. Jones, J. T. Gibbon, L. F. J. Piper, V. R. Dhanak, and T. D. Veal, *APL Mater.* **7**, 022528 (2019).
42. H. H. Tippins, *Phys. Rev.*, **140**, A316 (1965).
43. N. Ueda, H. Hosono, R. Waseda, and H. Kawazoe, *Appl. Phys. Lett.*, **71**, 933 (1997).
44. H. Peelaers and C. G. Van de Walle, *Phys. Stat. Solidi B*, **252**, 828 (2015).
45. C. Janowitz, V. Scherer, M. Mohamed, A. Krapf, H. Dwelk, R. Manzke, Z. Galazka, R. Uecker, K. Irmscher, R. Fornari, M. Michling, D. Schmeisser, J. R. Weber, J. B. Varley, and C. G. Van de Walle, *New Jour. of Phys.*, **13**, 085014 (2011).
46. J. Wu, W. Walukiewicz, K. M. Yu, J. W. Ager, E. E. Haller, H. Lu, W. J. Schaff, Y. Saito, and Y. Nanishi, *Appl. Phys. Lett.*, **80**, 3967 (2002).
47. I. Vurgaftman, J. R. Meyer, and L. R. Ram-Mohan, *J. Appl. Phys.*, **89**, 5815 (2001).
48. J. A. Van Vechten and T. K. Bergstresser, *Phys. Rev. B*, **1**, 3351 (1970).
49. N. Nepal, J. Li, M. L. Nakarmi, J. Y. Lin, and H. X. Jiang, *Appl. Phys. Lett.*, **87**, 242104 (2005).
50. R. E. Jones, R. Broesler, K. M. Yu, J. W. Ager III, E. E. Haller, W. Walukiewicz, X. Chen, and W. J. Schaff, *J. Appl. Phys.*, **104**, 123501 (2008).